

Analyst

Accepted Manuscript



This is an *Accepted Manuscript*, which has been through the Royal Society of Chemistry peer review process and has been accepted for publication.

Accepted Manuscripts are published online shortly after acceptance, before technical editing, formatting and proof reading. Using this free service, authors can make their results available to the community, in citable form, before we publish the edited article. We will replace this *Accepted Manuscript* with the edited and formatted *Advance Article* as soon as it is available.

You can find more information about *Accepted Manuscripts* in the [Information for Authors](#).

Please note that technical editing may introduce minor changes to the text and/or graphics, which may alter content. The journal's standard [Terms & Conditions](#) and the [Ethical guidelines](#) still apply. In no event shall the Royal Society of Chemistry be held responsible for any errors or omissions in this *Accepted Manuscript* or any consequences arising from the use of any information it contains.

ARTICLE

Controlled growth of polyhedral and plate-like Ag nanocrystals on nanofiber mat as SERS substrate

Cite this: DOI: 10.1039/x0xx00000x

Peng Jia, Jin Qu, Bing Cao, Yuxuan Liu, Chao Luo, Junhu An, Kai Pan*

Received 00th January 2012,

Accepted 00th January 2012

DOI: 10.1039/x0xx00000x

www.rsc.org/

We report a chemical deposition of silver nanocrystals (AgNCs) with different size and morphology, such as polyhedra and plates, on the polyacrylonitrile (PAN) nanofiber mat. High performance surface-enhanced Raman scattering (SERS) substrates are achieved. The effect of the experimental parameters, such as temperature, concentration and pH of $[\text{Ag}(\text{NH}_3)_2]\text{OH}$ aqueous solution, on the morphologies evolution and density of AgNCs are systematically investigated. The results suggest that the optimized nanofiber mat exhibits significant SERS performance with superior stability and reproduction, and the SERS enhancement factor (EF) can reach as high as 10^8 for 4-mercaptobenzoic acid (4-MBA). The optimized nanofiber mat also shows high SERS activity for p-aminothiophenol (4-ATP) over the whole nanofiber mat demonstrating the feasibility for detection of both analytes. The detection limit of 4-MBA and 4-ATP is as low as 10^{-9}M and 10^{-10}M respectively, making the nanofiber mat a promising candidate for SERS detection of chemical pollutants.

Introduction

Surface-enhanced Raman scattering (SERS) is recognized as one of the most sensitive spectroscopic tools, can provide the ultrasensitive detection of various biological and chemical species down to trace level and has potential applications in various fields.¹⁻⁵ Noble metallic nanostructures show excellent SERS activities due to their Surface Plasmon Resonance (SPR), which is arises from the collective oscillation of conduction electrons on the surface of metals and results in optical signal enhancement. Generally, Ag nanostructure has higher enhancement of Raman signal in the visible light region than other noble metals,⁶⁻⁸ and the size and morphology of AgNCs govern its optical and electronic property; thus, this has a great effect on the SERS property. SERS “hot spots” usually reside in the interstitial site consist of two or more coupled nanoparticles and metals with intersection, bifurcation and high radius of curvatures.⁹⁻¹¹ It is well known that “hot spots” make a major contribution to SERS, and the Raman intensity will be amplified by 10^3 - 10^{11} times when the analyte molecules are adsorbed around the “hot spot”.¹²⁻¹⁴ Therefore, it is crucial to prepare AgNCs with controlled size, density and morphology and manipulate the AgNCs assemblies to maximize SERS sensitivity.

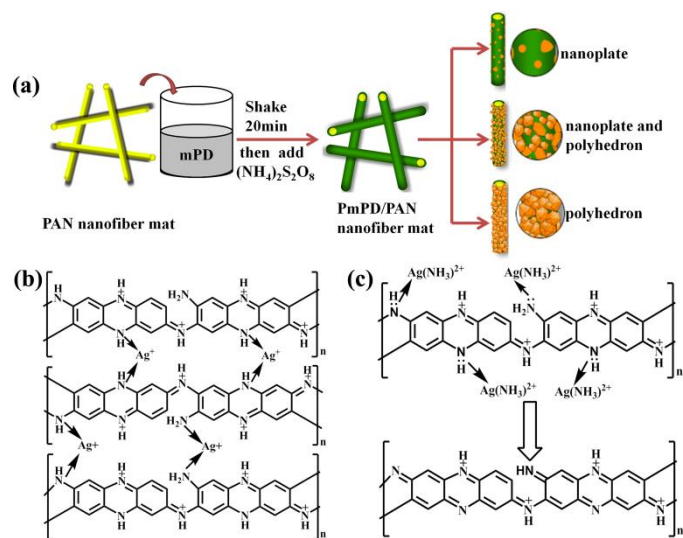
The generation of various substrates suitable for SERS have been established, such as aggregated Ag or Au colloids,¹⁵ metallic film over nanospheres,^{13,16} two-dimensional (2D) planar platforms¹⁷⁻¹⁹ and three-dimensional (3D) nanofibers assembled with noble metals.²⁰⁻²⁶ As an SERS substrate, nanofiber mat decorated with noble metallic structures has attracted a lot of attention because of its remarkable

characteristics such as flexibility, mechanical resilience and the possibility of large-scale preparation. In addition, the extremely large surface area to volume ratio might provide nanofibers with additional binding sites for absorbing analyte molecules, improving the sensitivity of the prepared substrate.^{27,28} The uniform and continuous three-dimensional (3D) nanofiber mat can be prepared by electrospinning, which is a very versatile and scalable technique.^{29,30}

The noble metals with different morphology, such as nanoparticles, nanorods, nanowires, and nanoplates, have attracted considerable interest in various fields, because of their potential applications in optics, catalysis, surface-enhanced Raman scattering (SERS) microelectronics and biological diagnostics.²¹⁻³⁵ The morphology of AgNCs has a great effect on their SERS performance. The Ag nanoplates and polyhedra demonstrate sharper corners, which create enormous “hot spots”. In this regard, the growth of Ag nanoplates and polyhedra on the nanofiber mat should be an effective approach to more flexible SERS substrates with a high density of “hot spots”. In addition, the size and density control of AgNCs for SERS effect is also important. Thus, it is necessary to control the size, morphology and density of AgNCs to obtain a highly active SERS substrate.

Here, we report a simple chemical deposition method to prepare flexible and highly sensitive SERS substrates via directly growing Ag nanoplates and polyhedra on PAN nanofibers, as shown in Scheme 1. The morphology, size and density of AgNCs can be controlled by changing a series of experimental parameters to obtain the highest SERS activity. The plate-like and polyhedral AgNCs-grafted PAN nanofiber mat provide not only abundant “hot spots” but also high surface area for absorbing plenty

of analyte molecules, thus rendering the high SERS sensitivity. We believe that the resultant nanofiber mat can serve as an SERS substrate with high sensitivity for the detection of chemical and biological analytes. Furthermore, noble metals attached to the conducting polymers are of particular interest, as this kind of composited material not only possesses processing advantages, but also shows excellent electronic properties.³⁶ Therefore, the prepared AgNCs@PAN-g-PmPD nanofiber mat can also be used in various electronic device applications.



Scheme 1. Schematic diagram showing the preparation of SERS active nanofiber decorated with AgNCs of different morphologies (a). Chelation of PmPD with Ag^+ (b). Reaction (c) of PmPD with $[\text{Ag}(\text{NH}_3)_2]\text{OH}$ aqueous solution.

Experiment section

Materials

Polyacrylonitrile (Mw=15,000), m-phenylenediamine (mPD), silver nitrate (AgNO_3) and p-aminothiophenol (4-ATP) were purchased from Sigma–Aldrich. Dimethyl Formamide (DMF) and ammonia were products of Beijing Chem. Co. (Beijing, China). 4-mercaptobenzoic acid (4-MBA) was provided by Alfa Aesar. All chemicals are of analytical grade and used as received without further purification.

Electrospinning PAN nanofiber

The PAN nanofiber was fabricated using the same method in our previous studies.^{37,38} PAN (4 g) was dissolved in the DMF (46 g) to make the polymer solution with a concentration of 8 wt%, and then kept the polymer solution stirring for 12 h at 60 °C to obtain a homogeneous solution. Then, the PAN solution was loaded into a syringe equipped with a blunt needle with a diameter of 0.7 mm to electrospin at a positive voltage of 15 kV. The distance between the needle and collector was 10 cm and the setting solution feed rate was 1.2 mL.h⁻¹.

PAN-g-PmPD nanofiber Preparation

According to the strategy shown in Scheme 1, the typical procedure for the preparation of PAN-g-PmPD core/shell nanofibers was as

follows: firstly, 2.16 g mPD and 2.36 g $(\text{NH}_4)_2\text{S}_2\text{O}_8$ were dissolved in 25 mL DI water, respectively. A piece of (4×4 cm) PAN nanofiber was immersed into mPD solution and then added $(\text{NH}_4)_2\text{S}_2\text{O}_8$ to start the polymerization. The reaction mixture was shaken at 100 rpm in a bath operated at 15 °C. The nanofiber membrane was taken out after 2 h, and washed with DI water repeatedly to remove the residual monomer. Finally, the obtained nanofiber mat was dried completely in a vacuum for 12 h.

Controlled growth of AgNCs

The procedure of controlled growth of AgNCs on PAN-g-PmPD nanofiber mats was as follows: The PAN-g-PmPD nanofiber mat was immersed in $[\text{Ag}(\text{NH}_3)_2]\text{OH}$ aqueous solution with different concentration, pH and temperature ranges for 24 h. The obtained nanofiber membrane was washed with DI water repeatedly and dried in vacuum for 12 h.

Characterization

The functional groups on the surface of the PAN and PmPD-modified nanofibers were detected by attenuated total reflections Fourier transform infrared (ATR-FTIR) spectrometry using a Perkin-Elmer spectrum RXI, and the resolution of 4 cm⁻¹. The surface chemical compositions of pristine PAN nanofibers and the modified nanofibers were analyzed by X-ray photoelectron spectroscopy (XPS) using Thermo Electron Corporation ESCALAB250 equipment with an Al K α X-ray source (1486.6 eV). The surface morphologies of the nanofiber mats were studied by Hitachi S-4700 scanning electron microscopy (SEM). X-ray diffraction (XRD) patterns were acquired with a single crystal XRD diffractometer (BrukerAXS D8 ADVANCE, Germany) using Cu K α (1.5406 Å) radiation. Raman spectra were obtained on a Renishaw Micro-Raman Spectroscopy System (Renishaw inVia) using a 633nm excitation laser (the excitation power of 0.17 mW, the exposure time was 1s). Before Raman spectral examination, the nanofiber mat was immersed into probe molecules ethanol solution with different concentrations. Then, they were washed with ethanol to remove residual probe molecules and dried in a vacuum oven.

Results and discussion

Preparation of PAN-g-PmPD nanofiber

Figure 1 (a) and (b) show the SEM images of the pure PAN and PAN-g-PmPD nanofibers. It can be observed that the average diameter of PAN nanofibers increased to about 300 nm after mPD polymerization on the surface of PAN nanofibers. The initial surface of PAN nanofibers is smooth; after polymerization, the surface of PAN nanofibers becomes coarse. The core/shell structure can be clearly seen in Figure 1 (d). Meanwhile, the thickness of PmPD is about 50 nm from TEM images.

ATR-FTIR was used to study the surface composition of PAN and PAN-g-PmPD nanofibers; the results are shown in Figure 1 (c). The broad adsorption peak between 3500 and 3000 cm⁻¹ is assigned to the stretching vibration of -NH-.³⁹⁻⁴¹ The two peaks around 1620 and 1500 cm⁻¹ represent the stretching mode of

quinoid imine and benzenoid amine units, respectively.³²⁻⁴⁴ The adsorption band at $\sim 1257\text{ cm}^{-1}$ is attributed to the C-N stretching vibration in the benzenoid amine units. These data are consistent with those of PmPD nanoparticles.^{45, 46} XPS is used to further study the surface compositions of the nanofibers. The N1s signal have one signal component at about 398.1 eV due to the C=N group from PAN chains.⁴⁷ For PAN-PmPD, as seen in Figure 1 (d), the peak at 399.2 eV and 400.2 eV and are attributed to -NH- and -NH₂ in the benzenoid amine units respectively, while the one at 401.2 eV is due to -N⁺= in the quinoid amine.⁴⁸ The molar content of -NH-, -NH₂ and -N⁺= is 69.5%, 24.7% and 6.2% respectively. All of the results confirm that the PmPD was successfully and uniformly coated on the surface of PAN nanofibers.

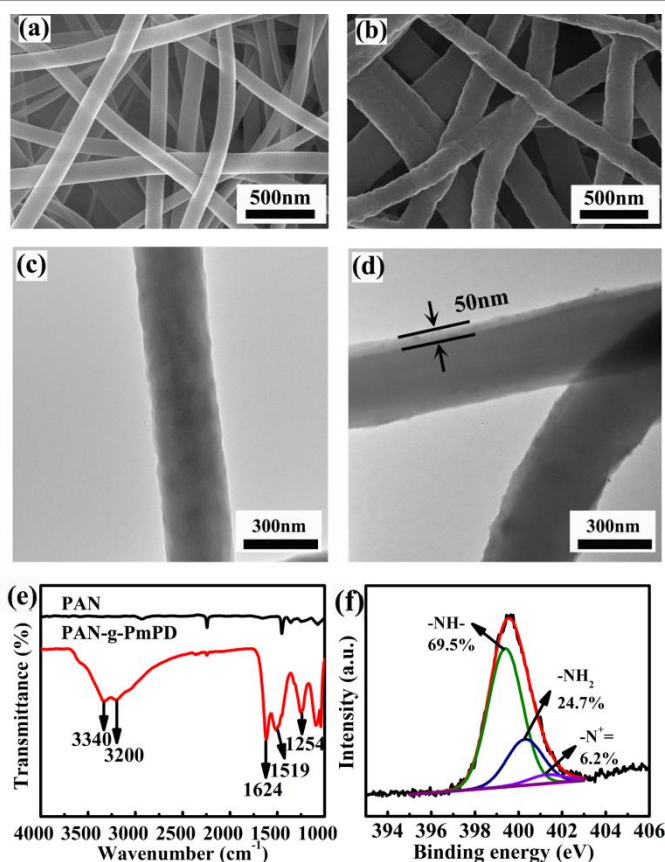


Figure 1. SEM and TEM images of the PAN nanofiber mat (a), (c) and PAN-g-PmPD nanofiber mat (b), (d); ATR-FTIR spectra of the PAN nanofiber and PAN-g-PmPD nanofiber (e); XPS N1s core-level spectra of the PAN-g-PmPD nanofiber mat (f).

Characterization of AgNCs@PAN-g-PmPD nanofiber

Figure 2 (a) and (b) show the typical SEM and TEM image of the PAN-g-PmPD nanofiber mat after the deposition of AgNCs. The surface of the nanofiber is completely covered by AgNCs which are uniformly attached to the nanofibers. The UV-vis adsorption spectra (Figure S1) also demonstrates the existence of AgNCs on the surface of PAN-g-PmPD nanofiber mat. The UV-vis spectrum of AgNCs@PAN-g-PmPD nanofiber displays a sharp adsorption peak at 312 nm, which

corresponds to the Plasmon resonance of Ag nanoparticles as being reported by others.⁴⁹ Figure 2 (c) and (d) shows the HRTEM images taken perpendicular to the flat faces of individual Ag nanoplate (marked by rectangle respectively in Figure 2 (b)). The HRTEM of Ag nanoplate shows the lattice spaces of 2.5 \AA can be assigned to the $1/3\{422\}$ plane, which is generally observed in silver or gold nanostructure in the form of thin plate.⁵⁰ Figure 2 (d) shows the HRTEM image and FFT image of Ag nanoplate by directing the electron perpendicular to their side space (marked by circle). The HRTEM results exhibit the stacking faults which are always observed in prismatic plate-like structure.⁵¹ The above results show that the PAN-g-PmPD nanofiber is fully covered by discal and polyhedral AgNCs, which will be very advantageous to form "hot spots".

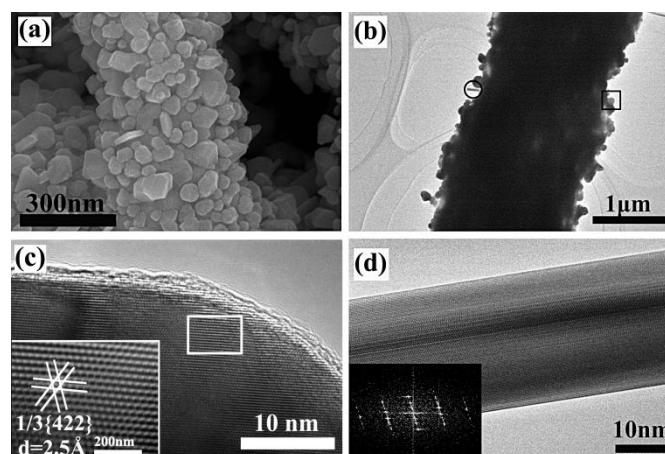


Figure 2. SEM image (a), TEM image (b) of AgNCs@PAN-g-PmPD nanofiber; HRTEM images taken perpendicular to the flat faces of individual Ag nanoplate (c) (the inset image is lattice-resolved TEM image taken from the corresponding marked area) and HRTEM image and the FFT image of Ag nanoplate by directing the electron perpendicular to their side space (d).

Mechanism of Ag nucleation and growth on PAN-g-PmPD nanofiber

It has been reported that conductive polymer and their copolymer can effectively adsorb metal ions via coordination and then reduce the as-absorbed metal ions in situ.⁵²⁻⁵⁸ For PmPD, benzenoid amine will transform into quinoid imine after the reaction.⁴⁸ $[\text{Ag}(\text{NH}_3)_2]^+$ has a much higher reduction potential than Ag^+ , and always acts as a weak oxidant. Therefore, we believe that the nucleation and growth of AgNCs have similar mechanism, as illustrated in Scheme 1.

To clarify the mechanism, PAN-g-PmPD nanofibers are characterized by XPS and XRD after reaction. As reported, the metallic Ag3d peaks centred at 373.9 and 367.9 eV, and Ag^+ exhibited two peaks at 375.8 and 369.6 eV.⁵⁹ Here (Figure 3 (c)), the Ag3d peaks appearing at 374.5 and 368.5 eV suggest that there are both metallic Ag and Ag^+ on the PAN-g-PmPD nanofibers. The molar content of metallic Ag is about 58.0%, and the Ag^+ on the nanofiber can be due to the complexation

between Ag^+ and imine. The XRD pattern also demonstrates the formation of metallic Ag (Figure S2); the sample's diffraction peaks can be well indexed to the (111), (200), (220), (311) and (222) crystal planes of Ag crystals.⁶⁰

Comparing with Figure 2 (f), the molar content of benzenoid amine (-NH- and -NH₂) decreases from 93.8% to 41.9% after reaction, which proves that the oxidation-reduction reaction is between benzenoid amine and $[\text{Ag}(\text{NH}_3)_2]^+$. The molar content of quinoid imine (-N= and -N⁺=) increases from 6.2% to 58.1% means the benzenoid amine transferring to quinoid imine during the oxidation-reduction reaction. In addition, an increase molar content of -N⁺= is found, indicating that imine took part in chelation.⁶¹

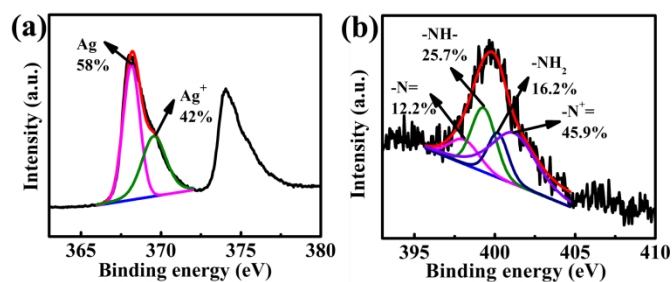


Figure 3. XPS N1s core-level spectral (a) and Ag3d_{5/2} core-level spectra (b) of AgNCs@PAN-g-PmPD nanofiber was prepared at the condition of pH=10.7, T=60 °C, c=10 g/L.

Controlled growth of Ag NCs

We divide the growth of silver crystals into three main stages: nucleation, evolution of nuclei into seed and growth seed into nanocrystals. The final shape of nanocrystals is determined primarily by the internal structure of the corresponding seed.⁶² It is well-known that crystal formation is dominated by both thermodynamic and kinetic factors. When the reaction is under thermodynamic control, the most stable single crystal seed will be produced. Because the low-index crystallographic facets of (111), (100) and (110) have increasing surface energy, the single-crystals are expect to exist as truncated octahedrons enclosed by a mix of (111) and (100) lattice plane to minimize the surface energy. When the reduction becomes slow enough, kinetic control will take over both nucleation and growth.⁶³ The atoms tend to form nuclei and seeds through random hexagonal close packing (rhcp), together with the inclusion of stacking faults, which can lead to the formation of plate seeds. The plate seed energy is extremely high because of the existence of stacking faults. As a result, the formation of plate seed can never be favored in terms of thermodynamics.⁶⁴ The formation of plate-like crystals can be achieved by slowing down reduction.

To observe the growth path of AgNCs on the PAN-g-PmPD nanofiber and to achieve the highest SERS intensity, temperature (T), $[\text{Ag}(\text{NH}_3)_2]\text{OH}$ aqueous solution's concentration (c) and pH are set as variables.

Figure 4 shows the morphologies the AgNCs@PAN-g-PmPD nanofiber mats obtained at different temperatures. Because of the considerably slow nucleation and growth process, only

plate-like crystals appear when the temperature is as low as 0 °C. As the temperature increase, Ag nanoplates and polyhedra can be found, and the surface coverage ratio of nanofibers increases at the same time. However, when the temperature reach to 90 °C, only polyhedra can be found and the particles tend to grow together. It is obvious that increasing the temperature enhances the reduction rate, which leads to the production of more seeds and promotes the AgNCs gradually becoming exclusively shaped as polyhedra.⁶⁵

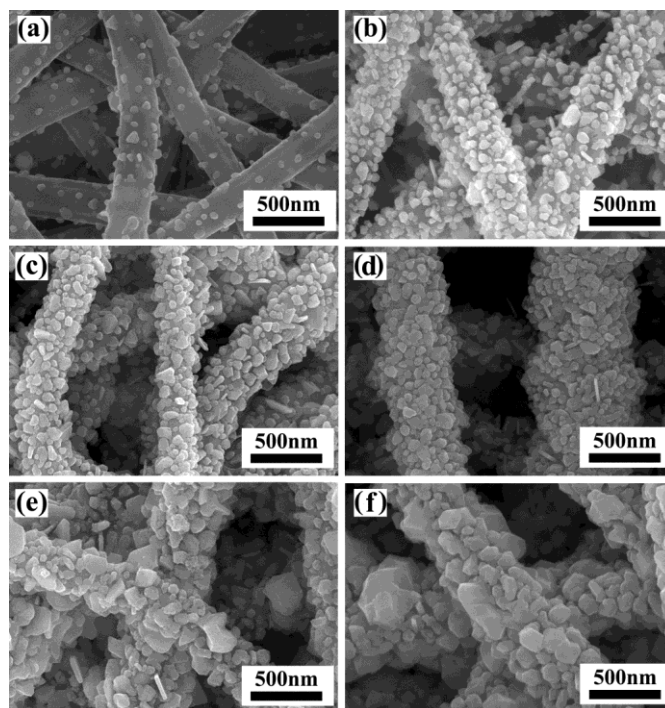


Figure 4. SEM images of AgNCs @ PAN-g-PmPD nanofiber fabricated under different temperatures: T=0 °C (a), T=30 °C (b), T=45 °C (c), T=60 °C (d), T=75 °C (e) and T=90 °C (f) (pH = 10.7, c=10 g/L, the growth process in 24h).

The pH of $[\text{Ag}(\text{NH}_3)_2]\text{OH}$ aqueous solution has a great effect on oxidation susceptibility. When the pH is too low, Ag^+ will not completely complex, and when the pH is too high, Ag^+ will excessively complex. Incomplete and excessive complexes will result in the reduced oxidation of $[\text{Ag}(\text{NH}_3)_2]\text{OH}$ aqueous solution. As shown in Figure 5 (a), (b), (c) and (d), the shape and size of AgNCs fabricated at different pH conditions are not significantly changed. However, the coverage ratio increases firstly and then decreases with the increasing pH value. If the pH is either too low or too high, the reaction rate is relatively slow, which reduces the amount of AgNCs.

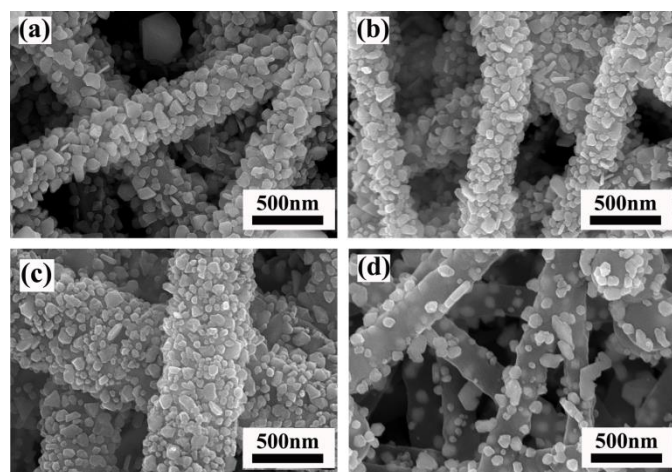


Figure 5. SEM images of AgNCs @ PAN-g-PmPD nanofiber fabricated under different pH value: 9.9 (a), 10.4 (b), 10.7 (c), 11.3 (d) ($c=10$ g/L, $T=60$ °C)

Figure 6 shows the morphologies of the AgNCs@PAN-g-PmPD nanofiber mats prepared at different concentrations of $[\text{Ag}(\text{NH}_3)_2]\text{OH}$ aqueous solution. When the concentration of $[\text{Ag}(\text{NH}_3)_2]\text{OH}$ aqueous solution increases from 5 g/L to 10 g/L (Figure 3 (c)), the crystal size changes a little, but the surface coverage ratio increases a lot. The crystal size increases to 100–150 nm without any change in coverage ratio when the concentration is 15 g/L. These results indicate that a higher concentration can produce more seeds and leads to much larger AgNCs and a higher coverage ratio.

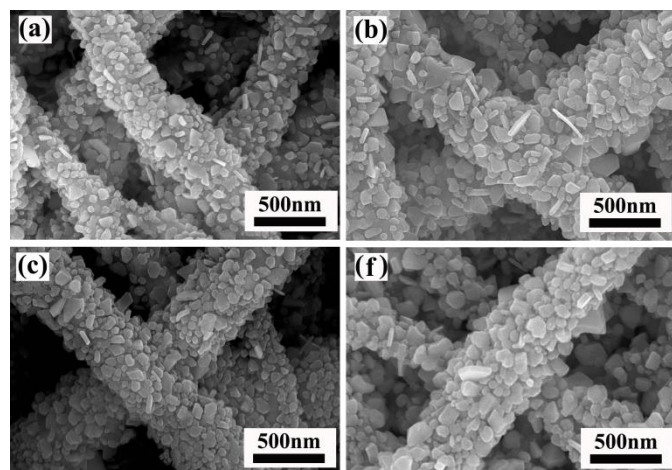


Figure 6. SEM images of AgNCs @ PAN-g-PmPD nanofiber fabricated under different concentration: 5 g/L (a), 7 g/L (b), 10 g/L (c) and 15 g/L (d) ($T=60$ °C, $\text{pH}=10.7$).

SERS property of AgNCs @ PAN-g-PmPD nanofiber mat

The obtained AgNCs@PAN-g-PmPD nanofiber mat possesses excellent mechanical flexibility, which can be folded into a hollow cylinder and tailored into any shape, as shown in Figure S3. The excellent flexibility ensures that the nanofiber mat will be a useful SERS active substrate for real applications. 4-MBA was used as a probe molecule to determine the optimized AgNCs@PAN-g-PmPD nanofiber mat and detects its SERS

activity and reproducibility. 4-MBA has distinct Raman features and is easy to be absorbed on the surface of AgNCs due to the existence of -SH. The main Raman peaks for 4-MBA are located at 1075 and 1590 cm^{-1} , which belong to the $\nu(\text{CC})$ ring breathing mode and stretching mode, respectively.⁶⁶ Figure 7 shows the SERS spectra and peak intensity of the AgNCs @ PAN-g-PmPD nanofiber mats obtained under different reaction conditions. All of the nanofiber mats are exposed to 10^{-4} M 4-MBA in ethanol. Both high temperature and high concentrations can elevate the reduction power of the system, leading to the yield of more AgNCs with smaller interspaces, and higher Raman intensity. However, AgNCs grow together when temperature reached to 90 °C, meaning that low Raman intensity will be observed because of the decreased interspaces among AgNCs. The Raman intensity decreases because of the reduced density of hot spots when the concentration increases to 15 g/L. When the pH is too low or too high, the reduction power of the system decreases, more likely yielding fewer AgNCs, resulting in larger interspaces. The nanofiber mat ($T=60$ °C, $\text{pH}=10.7$, $c=10$ g/L) shows the highest SERS intensity. Compared to other samples, nanofiber mats ($T=60$ °C, $\text{pH}=10.7$, $c=10$ g/L) has more suitable sizes and greater density which produced more Raman “hot spots”.

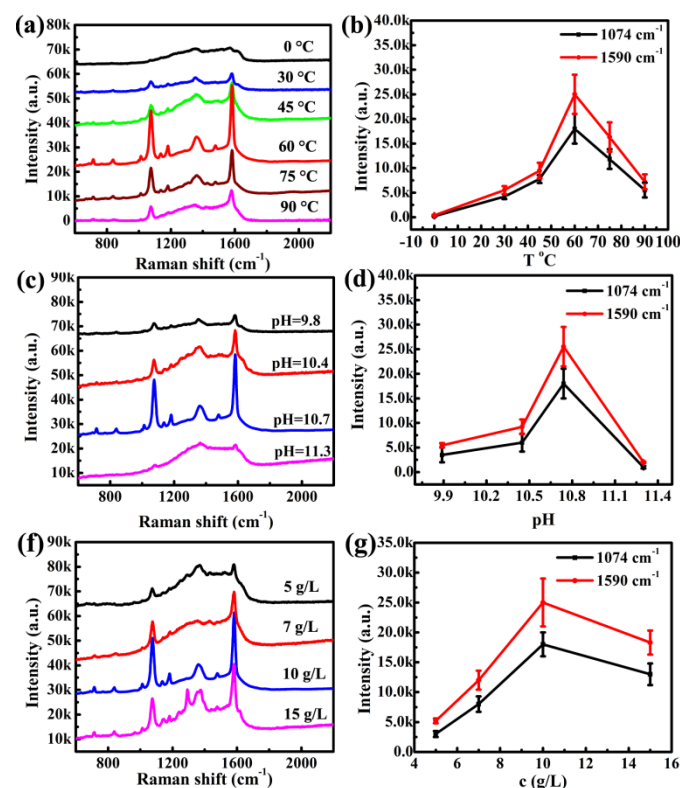


Figure 7. SERS spectra and peak intensity of 10^{-4} M 4-MBA adsorbed on the surface AgNCs@PAN-g-PmPD mat prepared at different T (a) and (b), pH (c) and (d), concentration (e) and (f).

To prove the sensitivity of AgNCs@PAN-g-PmPD nanofiber mats, the SERS spectra of 4-MBA are collected by varying the concentration from 10^{-4} M to 10^{-9} M. As shown in Figure 8 (a),

when the concentration of 4-MBA is as low as 10^{-8} M, the signal can be detected with this substrate. Further decrease the concentration of 4-MBA to 10^{-9} M, the Raman intensity will be comparable to the background noise, as shown in Figure S4. It is normal to find Raman signals will be strongly influenced by noise when the concentration of the analyte is too low.¹⁸ The enhancement factor (EF) can't be accurately calculated because of the rough surface of the nanofibers. Compared to similar Ag-nanofiber structures⁶⁷ an EF value of 10^7 - 10^8 can be roughly estimated.

Figure 8 (b) illustrates the corresponding plot of I_{SERS} versus $-\log[4\text{-MBA}]$, in which the I_{SERS} is the SERS intensity record for the band at 1075 cm^{-1} , which is the marker band in the 4-MBA spectrum. The results show that the data can be fitted by linear plot and the detection limit of 4-MBA is about 10^{-9} M, which is considered the lowest concentration leading to the SERS intensity of the bond at 1075 cm^{-1} . The capability of sensing 4-MBA at 10^{-9} M made the AgNCs@PAN-g-PmPD nanofiber mat a promising SERS active substrate for trace chemical detections.

The uniformity Raman signal is an essential parameter for reproducible SERS measurements. The uniformity of the obtained AgNCs@PAN-g-PmPD nanofiber mat was examined by randomly selecting twenty points on the substrate and recording their corresponding Raman spectra. Figure 8 (c) shows the intensity change of the Raman bands at 1075 cm^{-1} , which reveals excellent uniform response. The relative standard deviation (RSD) value of signal intensity of the Raman peak at 1075 cm^{-1} is observed below 0.1, revealing a good reproducibility across the entire area of the nanofiber mat. These results suggest that the obtained AgNCs@PAN-g-PmPD nanofiber mat has excellent stability and uniformity, which is very important in practical application, making the obtained nanofiber mat a promising SERS active substrate for trace chemical detections.

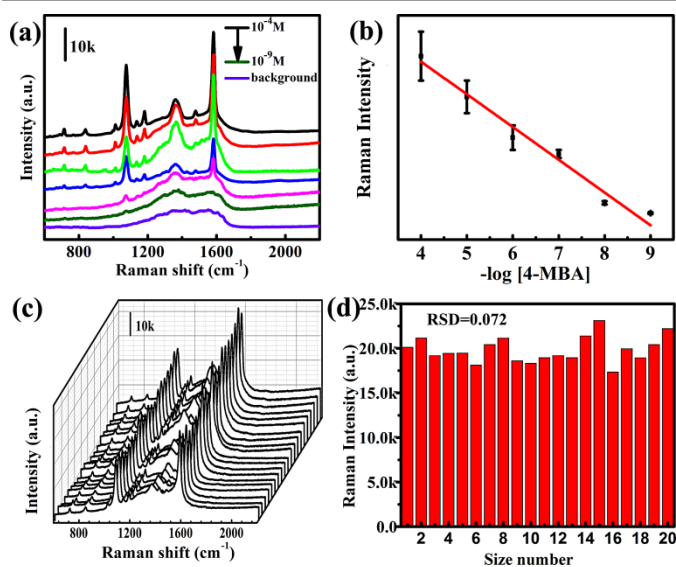


Figure 8. SERS spectral obtained from different concentration of 4-MBA using AgNCs@PAN-g-PmPD ($T=60\text{ }^{\circ}\text{C}$, $\text{pH}=10.7$,

$c=10\text{ g/L}$) substrate. [4-MBA]: from 10^{-4} M to 10^{-9} M (a); Relationship of Raman intensity at 1075 cm^{-1} and the concentration of 4-MBA. Uniform response (c) and RSD (relative standard deviation) (d) of the AgNCs@PAN-g-PmPD nanofiber mat probed with 10^{-4} M 4-MBA

To future reveal the SERS activity of the obtained AgNCs@PAN-g-PmPD nanofiber mat, SERS spectra of 4-ATP collected on the optimized AgNCs@PAN-g-PmPD nanofiber mat with different probe molecule concentrations (10^{-4} M- 10^{-10} M) are shown in Figure 9. The feature peaks of 4-ATP are located at $818, 1008, 1077, 1145, 1187, 1392, 1440$ and 1579 cm^{-1} which are consistent with reported values.⁶⁸ When the concentration 4-ATP are as low as 10^{-10} M signal can be detected with the SERS substrate demonstrating the feasibility for detection of both analytes on the optimized AgNCs@PAN-g-PmPD nanofiber mat. Figure 9 (b) shows the corresponding plot of I_{SERS} versus $-\log[4\text{-ATP}]$. The I_{SERS} is the SERS intensity record for the band at 1145 cm^{-1} , which is the marker band of 4-ATP. The results show that the data can be fitted by linear plot and the detection limit of 4-ATP is about 10^{-10} M. The trace detection of 4-MAB and 4-ATP make the optimized AgNCs@PAN-g-PmPD nanofiber mat a promising SERS substrate for the detection of chemical molecules.

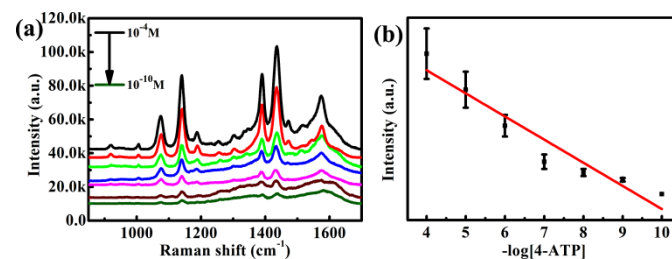


Figure 9. SERS spectra obtained from different concentration of 4-ATP using AgNCs@PAN-g-PmPD ($T=60\text{ }^{\circ}\text{C}$, $\text{pH}=10.7$, $c=10\text{ g/L}$) as SERS substrate. [4-ATP]: from 10^{-4} M to 10^{-10} M (a); Relationship of Raman intensity at 1145 cm^{-1} and the concentration of 4-ATP.

Conclusion

Polyhedral and plate-like AgNCs were generated on PAN-g-PmPD nanofibers by simple chemical deposition. The morphology and density of AgNCs could be controlled by changing experimental parameters such as temperature. The results demonstrated that the interspaces between AgNCs had a great effect on SERS performance, and the density of “hot spots” could be enlarged by increasing the amount of AgNCs throughout the nanofiber. The PAN-g-PmPD nanofiber almost fully covered by AgNCs showed the highest sensitivity in SERS detection of 4-MBA with a detection limit of up to 10^{-9} M. SERS spectra of 4-ATP collected on the optimized AgNCs@PAN-g-PmPD nanofiber mat future reveals the feasibility for detection of analyte. The obtained AgNCs@PAN-PmPD nanofibers showed excellent SERS sensitivity, reproducibility and flexibility, and thus could be used as a high SERS-active substrate with a wide range of applications.

Acknowledgement

The project is supported by the National Science Foundation of China (51373014) and Beijing Science and Technology Project (Z141100000914001).

Notes and references

^a Key laboratory of carbon fiber and functional polymers, Ministry of Education, Beijing University of Chemical Technology, Beijing, 100029, China.

^b College of Materials Science and Engineering, Beijing University of Chemical Technology, Beijing, 100029, China.

Electronic Supplementary Information (ESI) available: UV-Vis spectra of the PAN-g-PmPD nanofiber and the AgNCs@PAN-g-PmPD nanofiber; XRD pattern of AgNCs@PAN-g-PmPD nanofiber mat; The photograph of the AgNCs@PAN-g-PmPD nanofiber mat which was folded into a hollow cylinder and tailored into several pieces with any desired shape; SERS spectra of 10⁻⁹M 4-MBA adsorbed on the AgNCs@PAN-g-PmPD nanofiber mat and SERS spectra of the pure AgNCs@PAN-g-PmPD nanofiber mat.. See DOI: 10.1039/b000000x/

References

1. R. S. Golightly, W. E. Doering and M. J. Natan, *Acs Nano*, 2009, **3**, 2859-2869.
2. C. H. Lee, L. M. Tian and S. Singamaneni, *Acs Appl Mater Inter*, 2010, **2**, 3429-3435.
3. X. Fang and S. R. Ahmad, *Appl Phys B-Lasers O*, 2009, **97**, 723-726.
4. M. E. Stewart, C. R. Anderton, L. B. Thompson, J. Maria, S. K. Gray, J. A. Rogers and R. G. Nuzzo, *Chem. Rev.*, 2008, **108**, 494-521.
5. C. L. Haynes, A. D. McFarland, L. L. Zhao, R. P. Van Duyne, G. C. Schatz, L. Gunnarsson, J. Prikulis, B. Kasemo and M. Kall, *J Phys Chem B*, 2003, **107**, 7337-7342.
6. F. Yan and T. Vo-Dinh, *Sensor Actuat B-Chem*, 2007, **121**, 61-66.
7. J. N. Anker, W. P. Hall, O. Lyandres, N. C. Shah, J. Zhao and R. P. Van Duyne, *Nat Mater*, 2008, **7**, 442-453.
8. J. R. Kalluri, T. Arbneshi, S. A. Khan, A. Neely, P. Candice, B. Varisli, M. Washington, S. McAfee, B. Robinson, S. Banerjee, A. K. Singh, D. Senapati and P. C. Ray, *Angew Chem Int Edit*, 2009, **48**, 9668-9671.
9. E. Katz and I. Willner, *Angew Chem Int Edit*, 2004, **43**, 6042-6108.
10. M. L. Tran, S. P. Centeno, J. A. Hutchison, H. Engelkamp, D. Liang, G. Van Tendeloo, B. F. Sels, J. Hofkens and H. Uji-i, *J. Am. Chem. Soc.*, 2008, **130**, 17240-17273.
11. A. Courty, A. I. Henry, N. Goubet and M. P. Pileni, *Nat Mater*, 2007, **6**, 900-907.
12. F. S. Ou, M. Hu, I. Naumov, A. Kim, W. Wu, A. M. Bratkovsky, X. M. Li, R. S. Williams and Z. Y. Li, *Nano Lett*, 2011, **11**, 2538-2542.
13. Y. Fang, *Science*, 2008, **322**, 1790-1790.
14. M. Hu, F. S. Ou, W. Wu, I. Naumov, X. M. Li, A. M. Bratkovsky, R. S. Williams and Z. Y. Li, *J. Am. Chem. Soc.*, 2010, **132**, 12820-12822.
15. S. L. Kleinman, E. Ringe, N. Valley, K. L. Wustholz, E. Phillips, K. A. Scheidt, G. C. Schatz and R. P. Van Duyne, *J. Am. Chem. Soc.*, 2011, **133**, 4115-4122.
16. J. P. Camden, J. A. Dieringer, J. Zhao and R. P. Van Duyne, *Accounts Chem Res*, 2008, **41**, 1653-1661.
17. Y. Li, G. W. Lu, X. F. Wu and G. Q. Shi, *Journal of Physical Chemistry B*, 2006, **110**, 24585-24592.
18. J. Yan, X. J. Han, J. J. He, L. L. Kang, B. Zhang, Y. C. Du, H. T. Zhao, C. K. Dong, H. L. Wang and P. Xu, *Acs Appl Mater Inter*, 2012, **4**, 2752-2756.
19. S. K. Li, Y. X. Yan, J. L. Wang and S. H. Yu, *Nanoscale*, 2013, **5**, 12616-12623.
20. C. L. Zhang, K. P. Lv, H. T. Huang, H. P. Cong and S. H. Yu, *Nanoscale*, 2012, **4**, 5348-5355.
21. H. Zhu, M. L. Du, M. Zhang, P. Wang, S. Y. Bao, M. L. Zou, Y. Q. Fu and J. M. Yao, *Biosens. Bioelectron.*, 2014, **54**, 91-101.
22. C. H. Lee, L. M. Tian, A. Abbas, R. Kattumenu and S. Singamaneni, *Nanotechnology*, 2011, **22**, 275311-275318.
23. D. He, B. Hu, Q. F. Yao, K. Wang and S. H. Yu, *Acs Nano*, 2009, **3**, 3993-4002.
24. C. L. Zhang and S. H. Yu, *Chem Soc Rev*, 2014, **43**, 4423-4448.
25. C. L. Zhang, K. P. Lv, H. P. Cong and S. H. Yu, *Small*, 2012, **8**, 648-653.
26. J. Wang, H. B. Yao, D. A. He, C. L. Zhang and S. H. Yu, *Acs Appl Mater Inter*, 2012, **4**, 1963-1971.
27. A. G. Destaye, C. K. Lin and C. K. Lee, *Acs Appl Mater Inter*, 2013, **5**, 4745-4752.
28. C. Q. Chen, W. Li, C. Y. Cao and W. G. Song, *J Mater Chem*, 2010, **20**, 6968-6974.
29. W. Li, C. Y. Cao, C. Q. Chen, Y. Zhao, W. G. Song and L. Jiang, *Chem Commun*, 2011, **47**, 3619-3621.
30. C. Q. Chen, J. Qu, C. Y. Cao, F. Niu and W. G. Song, *J Mater Chem*, 2011, **21**, 5774-5779.
31. Y. Bao, C. L. Lai, Z. T. Zhu, H. Fong and C. Y. Jiang, *Rsc Adv*, 2013, **3**, 8998-9004.
32. Y. B. Zhao, A. H. Chen and S. Liang, *J Cryst Growth*, 2013, **372**, 116-120.
33. W. L. Barnes, A. Dereux and T. W. Ebbesen, *Nature*, 2003, **424**, 824-830.
34. L. A. Dick, A. D. McFarland, C. L. Haynes and R. P. Van Duyne, *J Phys Chem B*, 2002, **106**, 853-860.
35. N. L. Rosi and C. A. Mirkin, *Chem. Rev.*, 2005, **105**, 1547-1562.
36. A. H. Chen, H. Q. Wang and X. Y. Li, *Chem Commun*, 2005, **14**, 1863-1864.
37. J. Q. Wang, K. Pan, Q. W. He and B. Cao, *J. Hazard. Mater.*, 2013, **244**, 121-129.
38. J. Q. Wang, K. Pan, E. P. Giannelis and B. Cao, *Rsc Adv*, 2013, **3**, 8978-8987.
39. X. G. Li, M. R. Huang and Y. L. Yang, *Polymer*, 2001, **42**, 4099-4107.
40. L. Y. Chai, L. Y. Zhang, H. Y. Wang, W. T. Yu and P. L. Sang, *Mater Lett*, 2010, **64**, 2302-2305.
41. L. Y. Zhang, L. Y. Chai, H. Y. Wang and Z. H. Yang, *Mater Lett*, 2010, **64**, 1193-1196.
42. X. G. Li, M. R. Huang, W. Duan and Y. L. Yang, *Chem. Rev.*, 2002, **102**, 2925-3030.
43. M. R. Huang, H. J. Lu and X. G. Li, *J Mater Chem*, 2012, **22**, 17685-17699.

- 1
2
3
4
5
6
7
8
9
10
11
12
13
14
15
16
17
18
19
20
21
22
23
24
25
26
27
28
29
30
31
32
33
34
35
36
37
38
39
40
41
42
43
44
45
46
47
48
49
50
51
52
53
54
55
56
57
58
59
60
44. M. R. Huang, Q. Y. Peng and X. G. Li, *Chem-Eur J*, 2006, **12**, 4341-4350.
45. X. G. Li, M. R. Huang, P. Pan, Z. L. Zhu and Y. L. Yang, *Polym Degrad Stabil*, 2001, **71**, 333-341.
46. X. G. Li, R. Liu and M. R. Huang, *Chem Mater*, 2005, **17**, 5411-5419.
47. X. T. Wang, J. Q. Wang, R. Tsunashima, K. Pan, B. Cao and Y. F. Song, *Ind. Eng. Chem. Res.*, 2013, **52**, 2598-2603.
48. X. G. Li, X. L. Ma, J. Sun and M. R. Huang, *Langmuir*, 2009, **25**, 1675-1684.
49. X. L. Li, J. H. Zhang, W. Q. Xu, H. Y. Jia, X. Wang, B. Yang, B. Zhao, B. F. Li and Y. Ozaki, *Langmuir*, 2003, **19**, 4285-4290.
50. D. Jana and G. De, *J Mater Chem*, 2011, **21**, 6072-6078.
51. J. Zeng, J. Tao, W. Y. Li, J. Grant, P. Wang, Y. M. Zhu and Y. N. Xia, *Chem-Asian J*, 2011, **6**, 376-379.
52. X. G. Li, H. Feng and M. R. Huang, *Chem-Eur J*, 2010, **16**, 10113-10123.
53. X. G. Li, M. R. Huang and S. X. Li, *Acta Mater*, 2004, **52**, 5363-5374.
54. Q. F. Lü, M. R. Huang and X. G. Li, *Chem-Eur J*, 2007, **13**, 6009-6018.
55. M. R. Huang, Y. B. Ding and X. G. Li, *Analyst*, 2013, **138**, 3820-3829.
56. M. R. Huang, Y. B. Ding, X. G. Li, Y. Liu, K. Xi, C. L. Gao and R. V. Kumar, *Acs Appl Mater Inter*, 2014, **6**, 22096-22107.
57. M. R. Huang, X. W. Rao, X. G. Li and Y. B. Ding, *Talanta*, 2011, **85**, 1575-1584.
58. M.-R. Huang, H.-J. Lu and X. G. Li, *J. Colloid Interface Sci.*, 2007, **313**, 72-79.
59. V. G. Pol, D. N. Srivastava, O. Palchik, V. Palchik, M. A. Slifkin, A. M. Weiss and A. Gedanken, *Langmuir*, 2002, **18**, 3352-3357.
60. X. P. Sun, S. J. Dong and E. K. Wang, *Macromolecules*, 2004, **37**, 7105-7108.
61. O. P. Dimitriev, *Macromolecules*, 2004, **37**, 3388-3395.
62. Y. N. Xia, Y. J. Xiong, B. Lim and S. E. Skrabalak, *Angew Chem Int Edit*, 2009, **48**, 60-103.
63. Y. J. Xiong, I. Washio, J. Y. Chen, H. G. Cai, Z. Y. Li and Y. N. Xia, *Langmuir*, 2006, **22**, 8563-8570.
64. V. Germain, J. Li, D. Ingert, Z. L. Wang and M. P. Pileni, *J Phys Chem B*, 2003, **107**, 8717-8720.
65. J. M. Zhang, M. Fei and K. W. Xu, *Chinese Phys*, 2004, **13**, 1082-1090.
66. A. Michota and J. Bukowska, *J. Raman Spectrosc.*, 2003, **34**, 21-25.
67. L. F. Zhang, X. Gong, Y. Bao, Y. Zhao, M. Xu, C. Y. Jiang and H. Fong, *Langmuir*, 2012, **28**, 14433-14440.
68. Y. F. Huang, D. Y. Wu, H. P. Zhu, L. B. Zhao, G. K. Liu, B. Ren and Z. Q. Tian, *Phys. Chem. Chem. Phys.*, 2012, **14**, 8485-8497.